Available online at www.sciencedirect.com
SCIENCE DIRECT®
International Journal of Multiphase Flow 32 (2006) 344–364
International Journal of Multiphase Flow
www.elsevier.com/locate/ijmulflow

Large eddy simulation of droplet dispersion for inhomogeneous turbulent wall flow

I. Vinkovic [a,*], C. Aguirre [b], S. Simoëns [a], M. Gorokhovski [c]

[a] LMFA, UMR CNRS 5509, Ecole Centrale de Lyon, Université de Lyon I, INSA Lyon, 36 avenue Guy de Collongue, 69131 Ecully Cedex, France
[b] Universidad Nacional de Entre Rios, Parana, Entre-Rios, Argentina
[c] CORIA, UMR CNRS 6614, Université de Rouen, 76801 Saint Etienne du Rouvray Cedex, France

Received 14 April 2005; received in revised form 19 October 2005

Abstract

A large eddy simulation (LES) coupled with a Lagrangian stochastic model has been applied to the study of droplet dispersion in a turbulent boundary layer. Droplets are tracked in a Lagrangian way. The velocity of the fluid particle along the droplet trajectory is considered to have a large-scale part and a small-scale part given by a modified three-dimensional Langevin model using the filtered subgrid scale (SGS) statistics. An appropriate Lagrangian correlation timescale is considered in order to include the influences of gravity and inertia. Two-way coupling is also taken into account. The inter-droplet collision has been introduced as the main mechanism of secondary breakup. A stochastic model for breakup has been generalized for coalescence simulation, thereby two phenomena, coalescence and breakup are simulated in the framework of a single stochastic model. The parameters of this model, selectively for coalescence and for breakup, are computed dynamically by relating them to the local resolved properties of the dispersed phase compared to the main fluid. The model is validated by comparison with an agglomeration model and with experimental results on secondary breakup. The LES coupled with Lagrangian particle tracking and the model for droplet coalescence and breakup is applied to the study of the atmospheric dispersion of wet cooling tower plumes. The simulations are done for different droplet size distributions and volume fractions. We focused on the influence of these parameters on mean concentration, concentration variance and mass flux profiles.

Keywords: LES; Droplets; Coalescence; Breakup; Dispersion

1. Introduction

During the last decades, a good understanding of atmospheric dispersion has been achieved in neutral boundary layers as a result of numerical, laboratory and field investigations. Previous studies have focused

* Corresponding author. Tel.: +04 72 18 62 05; fax: +04 78 64 71 45.
E-mail address: ivana.vinkovic@ec-lyon.fr (I. Vinkovic).

0301-9322/$ - see front matter © 2005 Elsevier Ltd. All rights reserved.
doi:10.1016/j.ijmultiphaseflow.2005.10.005

on passive (Sykes and Henn, 1992), reactive (Sykes et al., 1992) and buoyant scalar dispersion. However, industrial stack emissions contain also particulate matter, as well as inertial particles and droplets. The aim of this research is the modeling and simulation of dispersion of droplets from elevated sources in atmospheric turbulent boundary layers. We will concentrate on the dynamical aspects, precisely on the impact of turbulence on the statistics of the dispersed phase. Interest will be drawn on the effect of turbulent coalescence on the evolution of the droplet size distribution and its impact on plume dispersion. In this study an Eulerian–Lagrangian approach is adopted. A LES with the dynamic subgrid scale model of Germano et al. (1991) is used to resolve the velocity field. The dispersed phase is computed with Lagrangian particle tracking. In addition to this, the LES is coupled with a Lagrangian stochastic model in order to take into account the SGS motion of particles. Finally, the coalescence and breakup of droplets are computed by a stochastic breakup/coalescence model based on the breakup model of Gorokhovski and Saveliev (2003) and its extension, developed in Apte et al. (2003). In our computations, two main distinctions from these works exist: (i) the formalism of breakup description is extended to the coalescence process; (ii) the main mechanism of droplet breakup is associated with inter-droplet collisions.

Since the pioneering work of Deardorff (1970), LES has become a well-established tool for the study of turbulent flows (Meneveau and Katz, 2000), the transport of passive scalars (Xie et al., 2004), the dispersion of reactive plumes (Meeder and Nieuwstadt, 2000) as well as the computation of particle-laden flows in a variety of conditions (Wang and Squires, 1996a; Fukagata et al., 1998; Shao and Li, 1999). The feasibility of LES to study preferential concentration of particles by turbulence (Wang and Squires, 1996b) and to compute flows with two-way momentum coupling (Boivin et al., 1998) has been reported. However, since relevant physical processes occur at unresolved scales (chemical reactions, droplet collisions and interactions, evaporation), the effect of the small scales on particle dispersion, motion or deposition must be modeled separately. The long term interest for using LES compared to Reynold averaged Navier–Stokes (RANS) approach is to obtain the instantaneous and local flow field structure which is necessary when passive scalars and chemical reactions play an important role. RANS cannot provide instantaneous solid particle or reactive scalar concentration peaks. Furthermore, the long term objective of this study is to apply the developed modeling tools to atmospheric dispersion as in Xie et al. (2004) and Meeder and Nieuwstadt (2000).

The Lagrangian stochastic approach has initially been proposed (Durbin, 1983; Thomson, 1987) in its natural context for modeling and prediction of turbulent diffusion and dispersion. In the framework of statistical RANS (Reynolds-averaged Navier–Stokes) description of turbulence, various random walk models for the diffusion of fluid particles and the dispersion of solid particles in two-phase flows have been proposed since then (Stock, 1996; Pozorski and Minier, 1998; Mashayek and Pandya, 2003, and references therein). The RANS computation with atomizing spray, modeled stochastically, was proposed in Gorokhovski (2001).

In this paper, the stochastic process for breakup was constructed as evolution towards the statistics when parent drop counts are no more correlated with product droplet counts. In our paper, a Lagrangian stochastic model is introduced in order to reconstruct the residual (subgrid scale) fluid velocity along particle trajectories. The stochastic model is written in terms of SGS statistics at a mesh level (Vinkovic et al., 2005a). In addition to this, an appropriate Lagrangian correlation timescale is considered in order to include the influences of gravity and inertia of droplets (Aguirre et al., 2004). In Aguirre et al. (2004) the correlation timescale is corrected due to the crossing trajectory effect (Csanady, 1963). Mainly, this means that the Lagrangian autocorrelation timescale is reduced and that the fluid particle at the previous position of the droplet is also tracked. Once the subgrid velocity of the fluid along the droplet trajectory reconstructed, droplet interactions are added to the numerical simulation. Mainly, this approach allows to obtain a complete and instantaneous velocity field containing the interesting turbulence properties such as the instantaneous large-scale turbulence structure movement influencing the timescale correlation and the turbulent kinetic energy.

Droplet coalescence is the process of droplet merging induced by their collision. Coalescence and growth of aerosol particles subject to a turbulent flow can modify completely the nature of plume dispersion. Turbulent fluctuations can induce relative motion between neighboring drops causing an enhancement of the collision rate. Moreover, because the dynamic response of each droplet is a sensitive function of its size and response time, turbulent coalescence can bias collision statistics causing substantial changes in the shape of the particle size distribution. When the liquid jet is issued from the injector into a turbulent gas flow, the fragments of different sizes are detached from the liquid bulk and accelerated by the gas flow and by the turbulent eddies

in the gas. These fragments undergo secondary breakup. Extensive measurement of airblast atomization in the liquid have been presented by Lasheras et al. (1998). It has been shown that starting from $x/D_g \sim 10$ in downstream direction (D_g being the diameter of the gas flow), up to $x/D_g \sim 25$–30, the Sauter diameter decreases significantly. Two physical scenarios of the secondary breakup may be considered in order to explain this effect: aerodynamic breakup and inter-droplet collisions. If we assume the first scenario, as the main mechanism of secondary breakup, then the droplets would be formed very quickly attaining their maximum stable size close to the injection region. Since the relative velocity between the gas and the newly produced droplets is significantly reduced, there will be no decrease in size of produced droplets in the downstream direction. At the same time, the breakup due to inter-droplet collisions (Georjon and Reitz, 1999) could explain the effect of significant streamwise decrease of the Sauter diameter. The relative velocity of fragments entrained by turbulence may be significant due to intermittency in the turbulent flow; the spray, in the region close to the injection, may be dense enough to induce this mechanism.

In the present work, the impact between droplets is a precursor of single coalescence/breakup model. According to properties of colliding droplets, the outcome of inter-droplet collisions is simulated stochastically with probabilities of droplet production over a large spectrum of size. Due to the complexity of the interaction between droplets, the coalescence and breakup phenomena are considered under scaling symmetry in variation of mother droplet size (in the case of breakup) or of droplet-collector size (in the case of coalescence). Based on the work of Kolmogorov (1941), this assumption has been introduced for atomization of liquids by Gorokhovski and Saveliev (2003). They showed that at high frequency of breakup events, the evolution of the PDF, in the space of radius, is governed by the special type of Fokker–Planck equation. This equation has been applied in our stochastic simulation of both breakup and coalescence phenomena, as described in Section 3. The main procedure has been inspired by the work done by Apte et al. (2003). The parameters of the model are obtained dynamically by relating them to the local resolved properties of the dispersed phase compared to the main fluid. Within each grid cell, mass conservation is applied. The results of the present model are compared with the model for micro-particle agglomeration of Ho and Sommerfeld (2002) and the experimental results on secondary breakup of Lasheras et al. (1998).

The LES coupled with the modified Langevin stochastic process at subgrid scales (Gardiner, 1985) and the model for droplet coalescence and breakup is applied to the study of the atmospheric dispersion of wet cooling tower plumes. Since we did not find any wind tunnel experiment or in-situ measurements of droplet dispersion in an atmospheric turbulent boundary layer, we compared the numerical results with the experiment on passive scalar plume dispersion of Fackrell and Robins (1982). The simulations are done for different droplet size distributions and volume fractions. Attention is paid on the influence of transport by turbulence, coalescence, droplet size distribution and volume fraction, on the statistics of the dispersed phase and on the behavior of the plume.

2. Simulation overview

2.1. Large eddy simulation (LES)

A turbulent boundary layer is computed using the LES code ARPS 4.5.2 (Xue et al., 2000; Xue et al., 2001). ARPS is a 3D, non-hydrostatic code where the fully compressible equations are solved with a time splitting procedure (Klemp and Wilhelmson, 1978). The continuity and momentum equations obtained by grid filtering the Navier–Stokes equations are

$$\begin{aligned} &\frac{\partial \tilde{u}_i}{\partial x_j} = 0, \\ &\frac{\partial \tilde{u}_i}{\partial t} + \tilde{u}_j \frac{\partial \tilde{u}_i}{\partial x_j} = -\frac{1}{\rho f}\frac{\partial \tilde{p}}{\partial x_i} + \frac{\partial}{\partial x_j}\left(v\left(\frac{\partial \tilde{u}_i}{\partial x_j} + \frac{\partial \tilde{u}_j}{\partial x_i}\right) - \tau_{ij}^r\right) + \tilde{B}_i, \end{aligned} \tag{1}$$

where u_i is the fluid velocity, p is the total pressure, v is the molecular kinematic viscosity, ρ_f is the density and $i = 1, 2, 3$ refers to the x (streamwise), y (spanwise), and z (normal) directions, respectively. B_i includes the

gravity and the Coriolis force. The tilde denotes application of the grid-filtering operation. The filter width $\tilde{\Delta}$ is defined as $\tilde{\Delta} = (\tilde{\Delta}_x\tilde{\Delta}_y\tilde{\Delta}_z)^{1/3}$, where $\tilde{\Delta}_x$, $\tilde{\Delta}_y$, $\tilde{\Delta}_z$ are the grid spacings in the x, y and z directions, respectively.

The effect of the subgrid scales on the resolved eddies in Eq. (1) is presented by the SGS stress, $\tau^r_{ij} = \widetilde{u_i u_j} - \tilde{u}_i\tilde{u}_j$.

The pressure equation is obtained by taking material derivative of the equation of state and replacing the time derivative of density by the velocity divergence using the mass continuity equation:

$$\frac{\partial\widetilde{\Delta p}}{\partial t} + \tilde{u}_j\frac{\partial\widetilde{\Delta p}}{\partial x_j} = \frac{\rho_f}{c^2}\left(\frac{1}{\tilde{\theta}}\frac{\partial\tilde{\theta}}{\partial t} - \frac{\partial\tilde{u}_i}{\partial x_i}\right), \tag{2}$$

where Δp is the pressure deviation from an undisturbed dry, hydrostatic base state, c is the speed of sound and θ is the potential temperature. The flow studied here is a neutral turbulent boundary layer. The potential temperature variations are therefore negligible.

The determination of the SGS stress, τ^r_{ij}, is parameterized using an eddy viscosity hypothesis:

$$\tau^r_{ij} - \frac{1}{3}\delta_{ij}\tau^r_{kk} = -2K_m\tilde{S}_{ij}, \tag{3}$$

where the turbulent eddy viscosity K_m is

$$K_m = C\tilde{\Delta}^2|\tilde{S}|, \tag{4}$$

the resolved-scale strain tensor is defined as

$$\tilde{S}_{ij} = \frac{1}{2}\left(\frac{\partial\tilde{u}_i}{\partial x_j} + \frac{\partial\tilde{u}_j}{\partial x_i}\right), \tag{5}$$

and $|\tilde{S}| = \sqrt{2\tilde{S}_{ij}\tilde{S}_{ij}}$ is the magnitude of $\tilde{S}_{ij}$. The model coefficient C in Eq. (4) is determined locally and instantaneously with the dynamic SGS closure developed by Germano et al. (1991) and modified by Lilly (1992).

The dimensions of the computational domain in the streamwise, spanwise and wall-normal directions are, respectively, $l_x = 6H$, $l_y = 3H$ and $l_z = 2H$, H being the boundary layer depth. The Reynolds number based on the friction velocity and the boundary layer depth is $Re = 15040$. The grid is uniform in the xy-planes and stretched in the z-direction by a hyperbolic tangent function. The grid spacings are $\Delta_x = 0.083H$, $\Delta_y = 0.083H$ and $0.0025H < \Delta_z < 0.083H$.

The no-slip boundary condition is applied at the wall. On the top of the domain and in the spanwise direction the mirror free-slip and the periodic boundary conditions are applied, respectively. In the streamwise direction, at the end of the domain the wave-radiation open boundary condition is used (Klemp and Wilhelmson, 1978) in order to allow waves in the interior of the domain to pass out freely through the boundary with minimal reflection. At the beginning of the domain, in the streamwise direction forcing is applied. The data set is obtained from the experimental results of Fackrell and Robins (1982).

2.2. Lagrangian particle tracking

The motion of particles with material densities large compared to the fluid is considered. In this regime the drag and gravity forces are substantially larger than the forces associated with virtual mass and history effects. The particle equation of motion can be expressed as

$$\begin{aligned}\frac{\mathrm{d}\vec{x}_\mathrm{p}(t)}{\mathrm{d}t} &= \vec{v}_\mathrm{p}(t),\\ \frac{\mathrm{d}\vec{v}_\mathrm{p}(t)}{\mathrm{d}t} &= \frac{\vec{v}(\vec{x}_\mathrm{p}(t),t) - \vec{v}_\mathrm{p}(t)}{\tau_\mathrm{p}}f(Re_\mathrm{p}) + \vec{g}.\end{aligned} \tag{6}$$

In Eq. (6), $\vec{v}_\mathrm{p}$ is the particle velocity, $\vec{v}(\vec{x}_\mathrm{p}(t),t)$ is the velocity of the fluid at the particle position and $\vec{g}$ is the acceleration of gravity. The particle relaxation time τ_p is given by

$$\tau_{\mathrm{p}} = \frac{\rho_{\mathrm{p}} d_{\mathrm{p}}^2}{18 \rho_f \nu}, \tag{7}$$

where the particle density is denoted by ρ_{p} and the diameter by d_{p}. Effects of nonlinear drag are incorporated through $f(Re_{\mathrm{p}})$ and in this work an empirical relation from Clift et al. (1978) is used:

$$f(Re_{\mathrm{p}}) = \begin{cases} 1 & \text{if } Re_{\mathrm{p}} < 1, \\ 1 + 0.15 Re_{\mathrm{p}}^{0.687} & \text{if } Re_{\mathrm{p}} \geqslant 1, \end{cases} \tag{8}$$

where

$$Re_{\mathrm{p}} = \frac{|\vec{v}_{\mathrm{p}} - \vec{v}| d_{\mathrm{p}}}{\nu} \tag{9}$$

is the particle Reynolds number.

The particle equation of motion 6 is time advanced using a second-order Runge–Kutta scheme. A fourth-order Runge–Kutta scheme has been tested and no differences were observed. The fluid velocity at the particle position $\vec{v}(\vec{x}_{\mathrm{p}}(t), t)$ is given by the velocity field of the LES, plus a subgrid contribution. The large-scale component of the fluid velocity at the particle position is obtained by a tri-linear quadratic Lagrange interpolation scheme with 27 nodes, as described by Casulli and Cheng (1992). The SGS contribution is determined by a modified Lagrangian stochastic model.

2.3. Stochastic modeling of the subgrid scale fluid velocity at particle position

2.3.1. Fluid particle

The SGS velocity of droplets is given by analogy with the SGS stochastic model for fluid particle dispersion (Vinkovic et al., 2005a). Namely, the Lagrangian velocity of the fluid particle is given by

$$v_i(t) = \tilde{u}_i(\vec{x}(t)) + v_i'(t). \tag{10}$$

This velocity is considered to have an Eulerian large-scale part $\tilde{u}_i(\vec{x}(t))$ (which is known) and a fluctuating SGS contribution $v_i'(t)$, which is not known and will be modeled by the stochastic approach. The movement of fluid elements at a subgrid level is given by a three-dimensional Langevin equation (Gardiner, 1985), originally proposed as a stochastic model for the velocity of a microscopic particle undergoing Brownian motion:

$$\begin{cases} \mathrm{d}v_i' = \alpha_{ij}(\vec{x}, t) v_j' \mathrm{d}t + \beta_{ij}(\vec{x}, t) \mathrm{d}\eta_j(t), \\ \mathrm{d}x_i = v_i \mathrm{d}t, \end{cases} \tag{11}$$

where $\mathrm{d}\eta_j$ is the increment of a vector-valued Wiener process with zero mean and variance $\mathrm{d}t$:

$$\begin{aligned} &\langle \mathrm{d}\eta_j \rangle = 0, \\ &\langle \mathrm{d}\eta_i \mathrm{d}\eta_j \rangle = \mathrm{d}t \delta_{ij}. \end{aligned} \tag{12}$$

The fluid particle velocity is given by a deterministic part $\alpha_{ij} v_j'$ and by a completely random part $\beta_{ij} \mathrm{d}\eta_j$. The coefficients α_{ij} and β_{ij} are determined by relating the subgrid statistical moments of $\vec{v}(t)$ to the filtered Eulerian moments of the fluid velocity, in analogy with van Dop et al. (1986) who developed this approach in the case of a classic Reynolds averaged decomposition. Knowing that the subgrid turbulence is homogeneous and isotropic at a mesh level (basic assumption of the LES), the velocity of fluid elements given by the Langevin model writes as

$$\mathrm{d}v_i' = \left(-\frac{1}{T_{\mathrm{L}}} + \frac{1}{2\tilde{k}} \frac{\mathrm{d}\tilde{k}}{\mathrm{d}t} \right) v_i' \mathrm{d}t + \sqrt{\frac{4\tilde{k}}{3T_{\mathrm{L}}}} \mathrm{d}\eta_i(t) \mathrm{d}t, \tag{13}$$

where T_{L} is the Lagrangian correlation timescale, given by

$$T_{\mathrm{L}} = \frac{4\tilde{k}}{3C_0 \tilde{\varepsilon}}, \tag{14}$$

$\tilde{k}$ being the subgrid turbulent kinetic energy, $\tilde{\varepsilon}$ the subgrid turbulent dissipation rate and C_0 the Lagrangian constant. The large-scale velocity of the fluid particle is directly computed by the LES with the dynamic Smagorinsky–Germano SGS model. An additional transport equation for $\tilde{k}$ is resolved. This equation is deduced from Deardorff (1980):

$$\frac{\partial \tilde{k}}{\partial t} + \tilde{u}_j \frac{\partial \tilde{k}}{\partial x_j} = \frac{K_m}{3} \frac{g}{\theta_0} \frac{\partial \tilde{\theta}}{\partial z} + 2K_m \tilde{S}_{ij}^2 + 2 \frac{\partial}{\partial x_j} \left(K_m \frac{\partial \tilde{k}}{\partial x_j} \right) - \tilde{\varepsilon}, \tag{15}$$

where $\tilde{\varepsilon} = C_\varepsilon \tilde{k}^{3/2} / \tilde{\Delta}$. The terms on the right-hand side of Eq. (15) correspond, respectively, to the production by buoyancy, the production by shear, the diffusion of $\tilde{k}$ and the dissipation. Since we are interested in neutral flows the potential temperature variation is neglected. The turbulent eddy viscosity K_m is computed by a dynamic procedure as described in the previous section. As suggested by Deardorff (1980), in the dissipation term, coefficient C_ε has the value:

$$C_\varepsilon = \begin{cases} 3.9 & \text{at first grid,} \\ 0.7 & \text{otherwise.} \end{cases} \tag{16}$$

The results of our simulations are very sensitive to the model constants (Eq. (16)). Dynamic closures for these constants could be introduced as suggested by Ghosal et al. (1995).

2.3.2. Fluid particle at droplet position

Because of its inertia effects and its different responses to gravity, droplets deviate from the fluid element that originally contained them, inducing a decorrelation. The main difficulty lies in the determination of the fluid particle velocity along the droplet trajectory, $\vec{v}(\vec{x}_p(t), t)$. This fluid velocity is computed with Eq. (10) and by analogy with Eq. (13) where T_L is replaced by T_L^p, a Lagrangian decorrelation timescale of the fluid velocity along the droplet trajectory. In order to account for gravity and inertia effects, we expect the modified timescale to be shorter than the fluid Lagrangian timescale T_L. The velocities to which a droplet is subjected will not be as well correlated as those to which a fluid particle is subjected. Moreover, as noted by Rodgers and Eaton (1990), a frequency measured in a Lagrangian frame is always smaller than a frequency measured in an Eulerian one. different forms have been previously developed for T_L^p, as Sawford and Guess (1991), Zhuang et al. (1989) for example. Aguirre et al. (2004) proposed the following formulation:

$$T_L^p = \frac{T_L}{\alpha_{grav} + \alpha_{inert}}, \tag{17}$$

where α_{grav} and α_{inert} are the coefficients related to gravity and inertia effects. The gravity effect is estimated following the approximation of Csanady (1963). Csanady (1963) proposed an interpolation between the Lagrangian correlation for vanishing inertia and small terminal velocity v_g and the Eulerian correlation for large v_g. In the direction parallel to gravity, with β an empirical constant, α_{grav} is given by

$$\alpha_{grav} = \sqrt{1 + \left(\frac{\beta v_g}{\tilde{\sigma}} \right)^2}, \tag{18}$$

where $\tilde{\sigma} = \sqrt{2\tilde{k}/3}$.

The inertia effect is evaluated in the limit of large inertia and vanishing v_g. A turbulent structure (length scale l), passing by a the moving particle would have a frequency of

$$\nu_{part} = \frac{|\vec{v}(\vec{x}_p(t), t) - (\vec{v}_p - \vec{v}_g)|}{\tilde{\epsilon}} \nu_L = \alpha_{inert} \nu_L, \tag{19}$$

where ν_L represents the Lagrangian correlation timescale.

For the limiting case, when gravity and inertia effects are negligible, the asymptotic behavior is satisfied. Recently, Shao (1995) and Reynolds (2000) have pointed out some contradictions relative to the structure function of $\vec{v}'(\vec{x}_p(t), t)$ and suggested that this velocity should be evaluated using a fractional Langevin equation. In fact, Wiener increments necessarily lead to a structure function proportional to dt when, in

the limiting case of large drift velocity and negligible inertia, the driving fluid velocity correlation approaches the Eulerian space–time correlation which is proportional to $dt^{2/3}$. However, the droplets studied here being far from these limiting cases, in a way identical to Reynolds (2000), we will forsake considerations of the structure function for increments in fluid velocity and treat $d\eta_j$ as increments of a Wiener process.

2.4. Two-way coupling

Influence of the presence of particles on the fluid motion has not yet been fully understood. In some cases, e.g. bubble flow, the presence of particles may produce velocity fluctuations of the surrounding fluid whose wavelength is smaller than the particle diameter.

However, it was numerically shown by Pan and Banerjee (1996) that the particles work as if they were an extra burden to the fluid when the particles are small and have much larger density than the surrounding fluid, as is the case in the present study. In such case, the momentum transfer from particles to fluid can be successfully modeled by adding the reaction force against the surface force acting on the particle to the Navier–Stokes equation, Eq. (1). This model is sometimes referred to as the force coupling model in contrast to the velocity coupling model (Pan and Banerjee, 1996) in which the velocity disturbance around the particle is considered.

When the two-way coupling is modeled by the force coupling model, an extra term appears in the transport equation of the subgrid turbulent kinetic energy, Eq. (15):

$$\widetilde{u'_k f'_k} = \frac{\rho_\mathrm{p} \Phi_\mathrm{p}}{\rho_f \tau_\mathrm{p}} \left(\widetilde{u'_k v'_k}(\vec{x}_\mathrm{p}(t), t) - \widetilde{u'_k v'_{pk}} \right) f(Re_\mathrm{p}), \tag{20}$$

where f'_k is the fluctuation component of the force from particles to fluid and Φ_p is the volume fraction in the grid cell occupied by the particles. Although several formulas have been proposed for the approximation of $\widetilde{u'_k v'_{pk}}$, the model by Porahmadi and Humphrey (1983)

$$\widetilde{u'_k v'_{pk}}(\vec{x}_\mathrm{p}(t), t) = \frac{2\tilde{k}}{1 + \tau_\mathrm{p}/T_\mathrm{L}} \tag{21}$$

has been adopted for simplicity. In addition to this, we assume that $\widetilde{u'_k v'_k}(\vec{x}_\mathrm{p}(t), t) = 2\tilde{k}$. Therefore, the additional term in the transport equation of the subgrid turbulent kinetic energy writes as

$$\widetilde{u'_k f'_k} = \frac{\rho_\mathrm{p} \Phi_\mathrm{p}}{\rho_f} \frac{2\tilde{k}}{\tau_\mathrm{p} + T_\mathrm{L}} f(Re_\mathrm{p}). \tag{22}$$

The coupling between the LES, the Lagrangian particle tracking, the modified Langevin model and the two-way coupling has been validated in comparison with wind tunnel experiments on sand particles. The results of these validations are shown in Vinkovic et al. (2005b) and Vinkovic (2005).

3. Coalescence and breakup model

In the dense spray regions, the new droplets are formed due to collisions between droplets. Some of collisions induce the breakup of droplets, others their coalescence. Although each individual outcome of inter-droplet interactions is a complex process, the number of breakup/coalescence events per unit time may be large. In this situation, it is natural to abstract a simple scenario of breakup/coalescence process and to represent its essential features. One of the possibilities is to assume that new droplets are formed under scaling symmetry; i.e. the size of mother drop (breakup), or of droplet-collector (coalescence) changes randomly and independently of its initial value. Considering, for example, the breakup process, the scaling symmetry assumption is $r \Rightarrow \alpha r$, where r is the size of the mother drop changed by an independent positive multiplier α ($0 < \alpha < 1$). This multiplier is random and governed by distribution $Q(\alpha)$, $Q(\alpha)d\alpha$ being the probability to get the produced droplet in the range $[\alpha; \alpha + d\alpha]$ of the mother droplet size. In addition to this

$$\int_0^1 Q(\alpha)\, d\alpha = 1. \tag{23}$$

This distribution is *in principle* unknown. If the frequency of breakup is high, Gorokhovski and Saveliev (2003) showed two universalities of such process. The first one is as follows: whatever the spectrum $Q(\alpha)$, the evolution of the PDF of radius $f(r, t)$, from its initial distribution $f(r_0)$ towards smaller sizes, is governed by a Fokker–Planck equation with two parameters. These two parameters are the first and the second logarithmic moments of $Q(\alpha)$, $\langle \ln \alpha \rangle$ and $\langle \ln^2 \alpha \rangle$. The second universality is: at last stages of breakup, the distribution of radius has power (fractal) behavior and only one parameter, the ratio $\langle \ln \alpha \rangle / \langle \ln^2 \alpha \rangle$, intervenes in the evolution of this distribution.

Using the same formalism, we formulate the coalescence process in the space of droplet-collector size relative to its possible maximal value. From the balance between gravity of droplets and their local inertia, we presume the upper limit of the radius, $r_{\max}$. Then we introduce the new variable $y = r_{\max} - r$, where r is the current radius of droplet-collector. Along with coalescence, the PDF $f(y, t)$ evolves from its initial shape $f(y_0)$ ($y_0 = r_{\max} - r_0$; r_0 being the initial radius of droplet-collectors) towards its distribution on smaller values of y; i.e. towards eventually maximum possible sizes of droplet-collector. We assume that after each coalescence

$$y \Rightarrow \beta y; \quad 0 < \beta < 1, \tag{24}$$

where β is a random multiplier governed by distribution $q(\beta)$; $q(\beta)\mathrm{d}\beta$ is the probability that after coalescence, the size of the collector, relative to its former size, can be found in the range $[\beta; \beta + d\beta]$ of its previous value $(r - r_{\max})$. The normalization of this distribution is

$$\int_0^1 q(\beta)\,\mathrm{d}\beta = 1. \tag{25}$$

The assumption (24) is equivalent to $\delta r = (1 - \beta)(r_{\max} - r)$, where δr is the increment of the collector size r. The distribution $q(\beta)$ is also an unknown function. However, it is clear that in the framework of scaling symmetry (24), the evolution of normalized distribution $f(y, t)$ will be governed by the same equations that have been derived by Gorokhovski and Saveliev (2003) for the fragmentation process. The parameters $\langle \ln \beta \rangle$ and $\langle \ln^2 \beta \rangle$ will be different from $\langle \ln \alpha \rangle$ and $\langle \ln^2 \alpha \rangle$. Similar to the closure proposed by Apte et al. (2003) for $\langle \ln \alpha \rangle$ and $\langle \ln^2 \alpha \rangle$, one may compute $\langle \ln \beta \rangle$ and $\langle \ln^2 \beta \rangle$ from the local resolved properties of gaseous and dispersed phases.

Droplets with a lifetime that attains the collision timescale are randomly selected by pairs of colliding partners within each grid cell. In the case of coalescence, the droplet of larger radius in each pair is called collector. The size of newly produced droplets is sampled from the analytical solution of the Fokker–Planck equation, selectively, either for y variable, $f(y, v_c t + 1)$ (giving new radius of droplet-collector, $r = r_{\max} - y$), if coalescence occurs, or for r variable, $f(r, v_c t + 1)$, in the case of breakup. The first case requires the knowledge of $\langle \ln \beta \rangle$ and $\langle \ln^2 \beta \rangle$, while the second one needs $\langle \ln \alpha \rangle$ and $\langle \ln^2 \alpha \rangle$. The choice between breakup and coalescence is based on the relative Weber number of colliding partners. The mass conservation is applied within each grid cell to compute the number of newly formed droplets. The velocities of these droplets are given by momentum conservation. The results of the present model are compared with the model for micro-particle agglomeration of Ho and Sommerfeld (2002) and the experimental results on secondary breakup of Lasheras et al. (1998).

3.1. Fokker–Planck equation for particle coalescence and breakup

In the case of breakup under the scaling symmetry with constant breakup frequency, the normalized distribution of newly produced droplets, $f(r, t)$, evolves according to the following integro-differential equation (Gorokhovski and Saveliev, 2003):

$$\frac{\partial f(r,t)}{\partial t} = v_c \int_0^1 f\left(\frac{r}{\alpha}, t\right) Q(\alpha) \frac{\mathrm{d}\alpha}{\alpha} - v_c f(r,t), \tag{26}$$

where v_c is the breakup frequency and

$$\int_0^\infty f(r,t)\,\mathrm{d}r = 1. \tag{27}$$

Expanding $\frac{1}{\alpha}f(\frac{r}{\alpha},t)$ on powers of $\ln\alpha$, one yields

$$\frac{1}{\alpha}f\left(\frac{r}{\alpha},t\right)=\sum_{n=0}^{\infty}(-1)^n\frac{1}{n!}\left(\frac{\partial}{\partial r}r\right)^n f(r,t)\ln^n\alpha. \tag{28}$$

With this expansion, Eq. (26) takes the following differential form:

$$\frac{1}{v_c}\frac{\partial f(r,t)}{\partial t}=-\frac{\langle\ln\alpha\rangle}{1!}\frac{\partial}{\partial r}rf(r,t)+\frac{\langle\ln^2\alpha\rangle}{2!}\frac{\partial}{\partial r}r\frac{\partial}{\partial r}rf(r,t)-\frac{\langle\ln^3\alpha\rangle}{3!}r\frac{\partial}{\partial r}r\frac{\partial}{\partial r}\frac{\partial}{\partial r}rf(r,t)+\cdots \tag{29}$$

Gorokhovski and Saveliev (2003) showed that although each term on the right-hand side of Eq. (29) can be significant, their renormalized sum of terms with $\langle\ln^k\alpha\rangle$, $k>2$ becomes, at large times, negligible. Then Eq. (29) reduces exactly to the Fokker–Planck equation, describing drift and diffusion of $f(r, t)$:

$$\frac{\partial f(r,t)}{\partial t}=-v_c\langle\ln\alpha\rangle\frac{\partial}{\partial r}(rf(r,t))+v_c\langle\ln^2\alpha\rangle\frac{\partial}{\partial r}r\frac{\partial}{\partial r}(rf(r,t)). \tag{30}$$

Here the first two logarithmic moments of $Q(\alpha)$, $\langle\ln\alpha\rangle$ and $\langle\ln^2\alpha\rangle$, are parameters of the model. The value of these two parameters will be fixed by the local dynamical properties of the flow and the dispersed droplets, as described in Section 3.5. The solution of Eq. (30) verifies to be

$$f(r,t)=\frac{1}{r}\int_0^{+\infty}\frac{1}{\sqrt{2\pi\langle\ln^2\alpha\rangle v_c t}}\exp\left\{-\frac{\left(\ln\frac{r}{R}-\langle\ln\alpha\rangle v_c t\right)^2}{2\langle\ln^2\alpha\rangle v_c t}\right\}f_0(R)\,\mathrm{d}R, \tag{31}$$

where $f_0(R)$ is the initial distribution before breakup or coalescence takes place. If the size of the primary droplet is supposed to be known, the initial distribution in Eq. (31) has the Dirac delta function shape, $f_0(R)=\delta(R-r_0)$. Then, Eq. (31) rewrites as

$$f(r,t)=\frac{1}{r}\frac{1}{\sqrt{2\pi\langle\ln^2\alpha\rangle v_c t}}\exp\left\{-\frac{\left(\ln\frac{r}{r_0}-\langle\ln\alpha\rangle v_c t\right)^2}{2\langle\ln^2\alpha\rangle v_c t}\right\}, \tag{32}$$

which is log-normal distribution with mean $\ln r_0+\langle\ln\alpha\rangle v_c t$ and variance $\langle\ln^2\alpha\rangle v_c t$.

Consider the coalescence process in the space of collector size relative to its maximal value. Introducing the distribution of droplet-collector, the rate of coalescence and scaling symmetry (24), one yields the evolution equation for normalized distribution $f(y, t)$ of the same form as Eq. (26):

$$\frac{\partial f(y,t)}{\partial t}=v_c\int_0^1 f\left(\frac{y}{\beta},t\right)q(\beta)\frac{\mathrm{d}\beta}{\beta}-v_c f(y,t). \tag{33}$$

Replacing r by y, and α by β in Eqs. (28)–(31), one rewrites for coalescence:

$$f(y,t)=\frac{1}{y}\frac{1}{\sqrt{2\pi\langle\ln^2\beta\rangle v_c t}}\exp\left\{-\frac{\left(\ln\frac{y}{y_0}-\langle\ln\beta\rangle v_c t\right)^2}{2\langle\ln^2\beta\rangle v_c t}\right\}, \tag{34}$$

where y_0 is addressed to the droplet-collector. In this work, the numerical procedure of breakup simulation given in Apte et al. (2003) will be extended by the choice of parameters v_c, $\langle\ln\beta\rangle$ and $\langle\ln^2\beta\rangle$. This allows to treat both breakup and coalescence with one model, and furthermore, to include naturally the contact between droplets.

3.2. General structure of the model

The domain is divided in square boxes. Their size is $L_{\mathrm{box}}=0.1$ m. In each box, at each time step, particles are randomly selected by pairs. The lifetime of droplets is 0 at the beginning of the simulation and increases on $\mathrm{d}t$ for each time step. If the lifetime of both selected droplets is bigger than $1/v_c$ and if the relative Weber

number, We_{rel}, of the selected droplets is smaller than the critical Weber number for coalescence, We_c, or bigger than the critical Weber number for breakup, We_b, new droplets are created. Their radius is sampled from distributions Eq. (32) or Eq. (34), selectively for breakup or coalescence. The size of collector gives y_0 in Eq. (34). The parent drops are replaced and Lagrangian tracking of newly formed droplets is continued till the next coalescence or breakup event. The velocities of the newly formed droplets result from the momentum balance and the velocities of the parent droplets as in Ho and Sommerfeld (2002). Note that neither coalescence nor breakup can occur if $We_c < We_{rel} < We_b$. In this case we consider that the droplets bounce apart.

3.3. Critical Weber number

For each pair of randomly selected particles, the relative Weber number is computed according to

$$We_{rel} = \frac{\rho_p v_{rel}^2 d_p}{\sigma}, \tag{35}$$

where $v_{rel} = |\vec{v}_{p,1} - \vec{v}_{p,2}|$ is the relative velocity between the droplets and σ the surface tension coefficient. This number describes the ratio of the inertial force to the surface tension force, which seem to be the main forces acting on the process for the studied cases. The relative velocity between droplets, v_{rel}, is considered rather than the relative velocity between the fluid and the droplet in order to take into account droplet contact for specific conditional cases.

When two droplets interact during flight, five different regimes of outcomes may occur (Kollár et al., 2005), namely (i) coalescence after minor deformation, (ii) bouncing, (iii) coalescence after substantial deformation, (iv) reflexive separation, and (v) stretching separation. The collision process is usually characterized by three parameters: the Weber number, the impact parameter, and the droplet size ratio. Boundary curves between regions of possible outcomes in terms of these parameters are proposed by several authors (Ashgriz and Poo, 1990; Brazier-Smith et al., 1972). Extensive experimental investigation was conducted and several outcome maps are presented in Qian and Law (1997). Further experimental studies were reviewed by Orme (1997).

Because we treat both coalescence and breakup we have to specify a critical Weber number for each process. In the present model, the critical Weber numbers for coalescence (We_c) and breakup (We_b) are fixed in comparison with the model for micro-particle agglomeration of Ho and Sommerfeld (2002) and the experimental results on secondary breakup of Lasheras et al. (1998). Then, the obtained values are compared with the experimental observation on the stream of droplets, cited above.

3.4. Collision frequency

Apte et al. (2003) did not model droplet coalescence. Thus, they have not considered particle contact. In the coalescence model by Sommerfeld (2001) droplet contact is taken into account. Therefore, in our model the contact frequency, necessary for both coalescence and breakup, is characterized following Sommerfeld (2001). The occurrence of coalescence and breakup is decided based on the collision frequency according to the kinetic theory of gases (Sommerfeld, 2001),

$$v_c = \frac{\pi}{4}(d_{p,1} + d_{p,2})^2 |\vec{v}_{p,1} - \vec{v}_{p,2}| n_p, \tag{36}$$

where n_p is the number of droplets per unit volume in the respective control volume, $d_{p,1}$ and $d_{p,2}$ are the droplet diameters and $v_{rel} = |\vec{v}_{p,1} - \vec{v}_{p,2}|$ is the instantaneous relative velocity between the two droplets.

3.5. Choice of parameters $\langle ln\,\alpha\rangle$, $\langle ln^2\,\alpha\rangle$, $\langle ln\,\beta\rangle$ and $\langle ln^2\,\beta\rangle$

Droplet coalescence and breakup are considered here as a discrete random process in the framework of uncorrelated events. By analogy with the stochastic model for secondary breakup of Apte et al. (2003), the parameters $\langle \ln\alpha\rangle$, $\langle \ln^2\alpha\rangle$, $\langle \ln\beta\rangle$ and $\langle \ln^2\beta\rangle$ are related to the local resolved properties of the dispersed phase, by

$$\begin{cases} \langle \ln \alpha \rangle = (\text{const}) \log\left(\frac{We_{\text{rel}_{\text{cr}}}}{We_{\text{rel}}}\right), \\ \frac{\langle \ln^2 \alpha \rangle}{\langle \ln \alpha \rangle} = \log\left(\frac{We_{\text{rel}_{\text{cr}}}}{We_{\text{rel}}}\right), \\ \langle \ln \beta \rangle = (\text{const}) \log\left(\frac{We_{\text{rel}}}{We_{\text{rel}_{\text{cr}}}}\right), \\ \frac{\langle \ln^2 \beta \rangle}{\langle \ln \beta \rangle} = \log\left(\frac{We_{\text{rel}}}{We_{\text{rel}_{\text{cr}}}}\right), \end{cases} \tag{37}$$

where 'const' is taken here of order of unity and $We_{\text{rel}_{\text{cr}}}$ is either We_{c} or We_{b}, whether coalescence or breakup takes place.

Apte et al. (2003) consider that breakup is generated by aerodynamic forces and that it occurs because of a high relative velocity between the gas and the droplet. In the present model, both coalescence and breakup are viewed as different outcomes of droplet collision events, Section 3.3, supported by Georjon and Reitz (1999) and the experiments on stream of droplets by Brazier-Smith et al. (1972), Ashgriz and Poo (1990) and Qian and Law (1997). Therefore, in the present model the parameters $\langle \ln \alpha \rangle$, $\langle \ln^2 \alpha \rangle$, $\langle \ln \beta \rangle$ and $\langle \ln^2 \beta \rangle$ are functions of the relative velocity between droplets (relative Weber number), and no longer of the relative velocity between the gas and droplet as in Apte et al. (2003).

4. Validation of the coalescence and breakup model

The Lagrangian model (Eq. (6)), the modified Langevin equation (Eqs. (13) and (17)) and the model for coalescence and breakup (Section 3.2) are tested in this section. In this part the LES is not applied and the mean properties of the flow field are obtained by analytic profiles. The instantaneous fluid velocity along the droplet trajectory is generated by the Langevin equation model described in Section 2.3.2. Two test cases are considered to validate the developed coalescence and breakup model: the model for micro-particle agglomeration of Ho and Sommerfeld (2002) and the experimental results on secondary breakup of Lasheras et al. (1998). For each simulation a relative critical Weber number, $We_{\text{rel}_{\text{cr}}}$, has to be fixed both for coalescence and breakup. Thereby, the complete model for coalescence and breakup is applied for each of the chosen cases presented below. Explicitly, both coalescence and breakup are active during each simulation.

4.1. Comparison with the stochastic model for micro-particle agglomeration (Ho and Sommerfeld, 2002)

The first test case considered to validate the developed coalescence and breakup model is a homogeneous isotropic turbulence field in a cube with periodic boundary conditions. The turbulence characteristics and the particle properties are summarized in Table 1. At the beginning of our simulation there are around 38,400 droplets in the domain, while at the end about 20,200 droplets remain.

Ho and Sommerfeld (2002) developed an agglomeration model. It relies for a given droplet, on the generation of a fictitious collision partner and the calculation of the collision probability according to the kinetic theory of gases related to the trajectory of the chosen droplet. The fictitious particle size is stochastically

Table 1
Turbulence characteristics and particle phase properties

Turbulent kinetic energy	$k = 0.001$–$0.25\ \text{m}^2/\text{s}^2$
Turbulent dissipation rate	$\varepsilon = 50\ \text{m}^2/\text{s}^3$
Kinematic viscosity	$\nu = 1.5 \times 10^{-5}\ \text{m}^2/\text{s}$
Turbulent integral timescale	$T_{\text{L}} = 6.5 \times 10^{-4}$–$1.6 \times 10^{-3}\ \text{s}$
Reynolds number	$Re_\lambda = 0.05$–8.5
Particle diameter	$d = 1.0$–$100\ \mu\text{m}$
Particle material density	$\rho_p = 1000\ \text{kg/m}^3$
Particle relaxation time	$\tau_{\text{p}} = 0.62$–$14\ \text{ms}$
Particle volume fraction	1.4×10^5

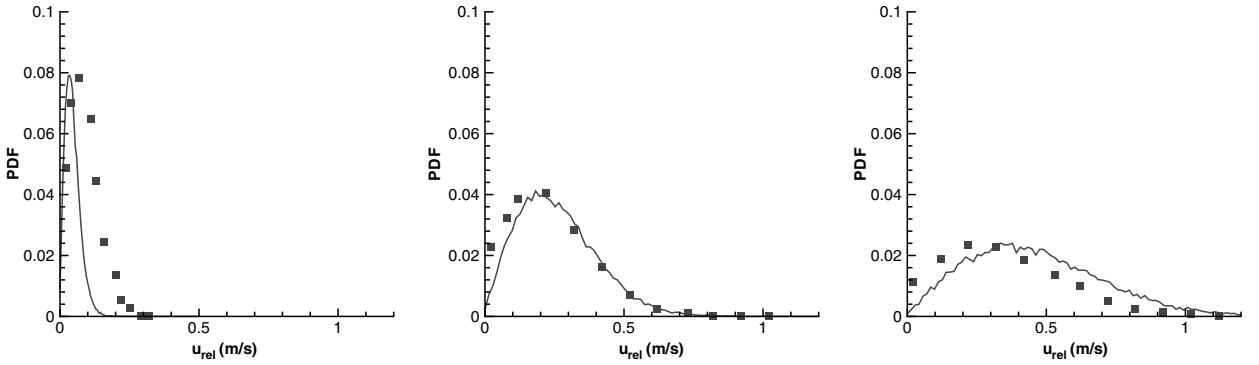

Fig. 1. Probability density function of the relative velocity between colliding droplets for different turbulent kinetic energy: line, present model; squares, Ho and Sommerfeld (2002); left, $k = 0.01\ \mathrm{m^2/s^2}$; center, $k = 0.1\ \mathrm{m^2/s^2}$; right, $k = 0.25\ \mathrm{m^2/s^2}$.

sampled from the local particle size distribution. If an agglomerate is formed, the properties of the new particle are directly determined by mass and momentum conservation of the colliding particles. For droplet transport, Ho and Sommerfeld (2002) use a Langevin equation model.

The PDF of the relative velocity between droplets for three different values of the turbulent kinetic energy obtained by our simulations are illustrated in Fig. 1. This PDF is obtained from all the droplets inside the domain. The results of our simulations are in good agreement with the model of Ho and Sommerfeld (2002). However, discrepancies exist for small values of the turbulent kinetic energy, when the rate of collision is small. The differences are probably due to the fact that in our model particles are randomly selected by pairs (as described in Section 3.2) while Ho and Sommerfeld (2002) generate fictitious collision partners. With rising turbulence level the relative velocity distribution is broadened towards higher values.

The time evolution of the size distribution of droplets is shown in Fig. 2. Even though our approach is completely different from the model of Ho and Sommerfeld (2002), both results are in close agreement. The initial size distribution is Gaussian with a mean diameter of 8 μm and a standard deviation of 2.5 μm. The turbulent kinetic energy is low and breakup does not take place. The number of small particles decreases rapidly in time due to coalescence. On the other hand, the number of large particles increases at a much lower rate because of the small volume equivalent diameter of small particles.

The critical relative Weber number for coalescence was fixed to $We_{\mathrm{rel_{cr}}} = We_{\mathrm{c}} = 1.25 \times 10^{-3}$. The experiments on the stream of droplets (Section 3.3) were mostly conducted for relative Weber numbers between 1 and 100. This is mostly due to the difficulty of generating streams of droplets with diameters smaller than 100 μm. However, $We_{\mathrm{c}} = 1.25 \times 10^{-3}$ is equivalent to choosing a critical relative velocity, $v_{\mathrm{rel_{cr}}} = 0.15\ \mathrm{m/s}$ for droplets of $d_{\mathrm{p}} = 8\ \mu\mathrm{m}$ in diameter, since $We_{\mathrm{rel_{cr}}} = \rho_{\mathrm{p}} v^2_{\mathrm{rel_{cr}}} d_{\mathrm{p}}/\sigma$. In their model, Ho and Sommerfeld (2002) use a critical relative velocity. Ho and Sommerfeld (2002) suppose that the formation of an agglomerate from two colliding particles takes place when the normal relative velocity between them is less than the critical velocity. This velocity is obtained from an energy balance when only the van der Waals forces are considered. For particles with a diameter of $d_p = 8\ \mu\mathrm{m}$, Ho and Sommerfeld (2002) find that $v_{\mathrm{rel_{cr}}} \sim 0.13\ \mathrm{m/s}$, which is practically the same value as the one used in our model.

4.2. Comparison with experimental results of Lasheras et al. (1998)

By mean of high-speed flow visualizations and phase droplet particle sizing techniques, Lasheras et al. (1998) examined the near- and the far-field breakup and atomization of a water jet by a high-speed annular air jet. They noted that the droplet diameter does not decrease to an asymptotic value at large downstream distances from the nozzle. The mean diameter decreases first, reaching a minimum, and then increases monotonically with distance from the nozzle. Lasheras et al. (1998) also observed that the minimum mean droplet diameter and its downstream position decrease with increasing air flow. Because it presents a mixed case of coalescence and breakup, this experiment is used as the second test case.

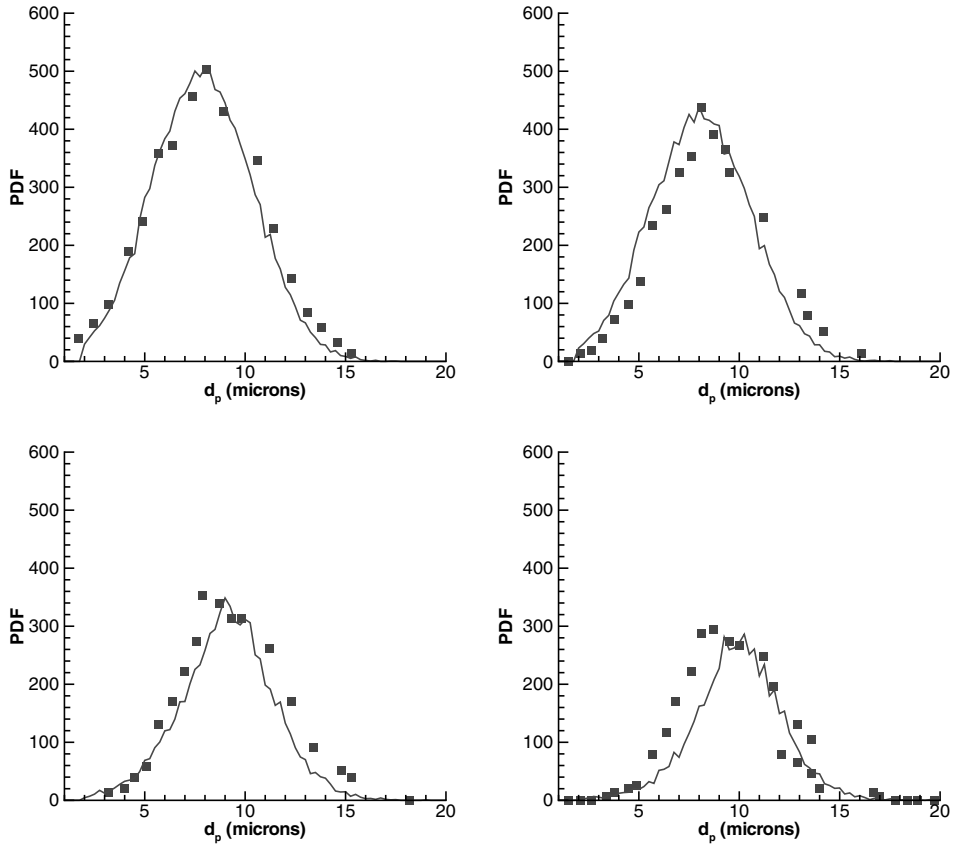

Fig. 2. Size distribution of particles undergoing coalescence at $t = 0$ s, $t = 1$ s, $t = 3$ s and $t = 5$ s: line, present model; squares, Ho and Sommerfeld (2002).

Table 2
Turbulence characteristics and particle phase properties

$U_{l_1} = 0.13$ m/s	$x_0 = 10D_g$	$d_{init} = 40$ μm	$m = 0.38$	$\varepsilon_{ad} = 0.72$	$k_{ad} = 0.72$
$U_{l_2} = 0.20$ m/s	$x_0 = 12D_g$	$d_{init} = 50$ μm	$m = 0.58$	$\varepsilon_{ad} = 0.63$	$k_{ad} = 0.63$
$U_{l_3} = 0.31$ m/s	$x_0 = 12D_g$	$d_{init} = 52$ μm	$m = 0.91$	$\varepsilon_{ad} = 0.52$	$k_{ad} = 0.52$

Different flow conditions were tested and they are summarized in Table 2. U_l is the liquid jet velocity. The subscripts l_1, l_2 and l_3 stand for three different initial liquid jet velocities. D_l is the liquid jet diameter. The rate of dissipation and the turbulent kinetic energy are normalized by the gas phase velocity U_g, the diameter of the gas phase jet D_g and the mass rate m according to

$$\varepsilon \approx \frac{U_g^3}{D_g(1+m)}, \tag{38}$$

where

$$m = \frac{\rho_l U_l D_l^2}{\rho_g U_g D_g^2}. \tag{39}$$

Since we are only interested in modeling secondary breakup, the model was applied at a downstream distance x_0 from the nozzle, where the primary breakup was over. For the initial droplet diameter a Gaussian PDF is

used, with a mean diameter, d_{init}, estimated from the mean Sauter diameter measured by Lasheras et al. (1998) at x_0. The mean Sauter diameter is given by

$$d_{\text{sauter}} = \frac{\sum_{i=1}^{N_p} d_{p,i}^3}{\sum_{i=1}^{N_p} d_{p,i}^2}, \tag{40}$$

where N_p is the total number of droplets in the domain. It is defined as the diameter of a droplet having the same volume/surface ratio as the entire spray. The time step used in the simulations is $dt = 5.6 \times 10^{-3}$ s. At each time step about 30,000 particles are tracked.

Fig. 3 shows the variation of the mean Sauter diameter with downstream distance for three different air flow rates. The results of our model are in good agreement with the experimental results of Lasheras et al. (1998). The model reproduces the transition between the breakup and the coalescence regions. The evolution of the mean Sauter diameter shows a non-monotonic dependence on x/D_g, first decreasing and then increasing. The value of the minimum droplet diameter and its location increase with increasing U_l.

As for the first test case the critical Weber numbers for breakup and coalescence are fixed in order to fit the experimental results. The critical relative Weber number for coalescence is fixed to $We_c = 0.7$. This is in accordance with the experimental observations on the stream of droplets (Brazier-Smith et al., 1972; Ashgriz and Poo, 1990; Qian and Law, 1997). The critical relative Weber number for breakup is fixed to $We_b = 1$ which is a very low value. However, in the experiments of Lasheras et al. (1998), there is a big uncertainty on the estimation of the turbulent dissipation rate and the turbulent kinetic energy at the centerline of the jet. By choosing a higher turbulent kinetic energy we could have obtained the same results with higher critical relative Weber numbers.

It should be mentioned that, the simulations carried out here are not in the same regime as the experiments of Brazier-Smith et al. (1972), Ashgriz and Poo (1990) or Qian and Law (1997). However, no other experiments containing a complete data set on the droplet dynamics were found. Clearly, the relative critical Weber number parameterized by different regimes remains an open question.

It is interesting to note here that breakup and coalescence take place at different stages of the coaxial jet.

In this study we are mostly interested in atmospheric dispersion of droplets. In atmospheric conditions, mean relative velocities are low and droplet collisions lead mostly to coalescence or bouncing rather than fragmentation. Therefore, the relative critical Weber number fixed in the first test case is used in the next section.

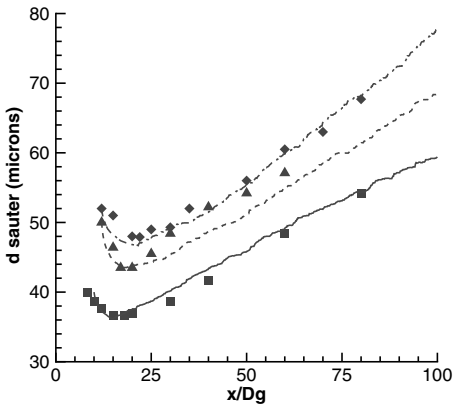

Fig. 3. Downstream variation of the Sauter mean diameter at the centerline of the jet: lines, present model; symbols, Lasheras et al. (1998); full line and squares, $U_{l_1} = 0.13$ m/s; dashed line and triangles, $U_{l_2} = 0.20$ m/s; dashed–dotted line and diamonds $U_{l_3} = 0.31$ m/s.

5. Application to the study of wet cooling tower plumes

The LES coupled with Lagrangian particle tracking and the model for droplet coalescence and breakup is applied to the study of the atmospheric dispersion of wet cooling tower plumes. Since we did not find any wind tunnel experiment or in situ measurements of droplet dispersion in an atmospheric turbulent boundary layer we compared the numerical results with the experiment on passive scalar plume dispersion of Fackrell and Robins (1982). Details about the setup and the LES of this case may be found in Vinkovic et al. (in press).

5.1. Simulation description

Inside water cooling tower plumes, the droplet size distribution can be characterized by a mean droplet diameter of 12 μm, a standard deviation of 4 μm and a concentration of 200 droplets/cm^3, Hodin et al. (1980). Droplets with an initial Gaussian size distribution of mean d$p = 12$ μm and variance 4 μm are injected at the source.

A full description of the experimental facility and results can be found in Fackrell and Robins (1982). Here, the main characteristics of the experiment necessary for understanding the simulations are given. A turbulent boundary layer over a rough wall is generated in an open-circuit wind tunnel. The height H of the turbulent boundary layer is 1.2 m and the roughness length is $z_0/H = 2.4 \times 10^{-4}$. The mean velocity at the boundary layer edge U_e is 4 m/s and the friction velocity $u_*/U_e = 0.047$. A passive scalar plume from a point source at $z_s/H = 0.19$ is studied. The elevated source has a 8.5 mm diameter and it emits at the average velocity of the flow over its height. The source gas consists only of a neutrally buoyant mixture of propane and helium. The former is used as a trace gas for concentration measurements. Fackrell and Robins (1982) measured the mean concentration, the concentration fluctuations and the fluxes in the passive scalar plume.

5.2. Results and analysis

The LES coupled with the subgrid stochastic model has already been applied to the study of passive scalar dispersion (Vinkovic et al., in press). Details of the boundary layer flow such as mean velocity, turbulent kinetic energy and fluctuation profiles can be found in Vinkovic et al. (in press). Here we will only describe the results relative to droplet dispersion.

The mean concentration profiles for droplets of 12 μm of 60 μm in mean diameter at different stations compared to the mean concentration profiles of passive scalar are shown in Fig. 4. Both types of droplets fall to the ground faster than the passive scalar plume. At the last station, droplets of 12 μm remain suspended while 60 μm droplets present a maximum concentration at the ground. The mean concentration profile of 60 μm droplets is no longer similar to the mean concentration profile of a passive scalar plume.

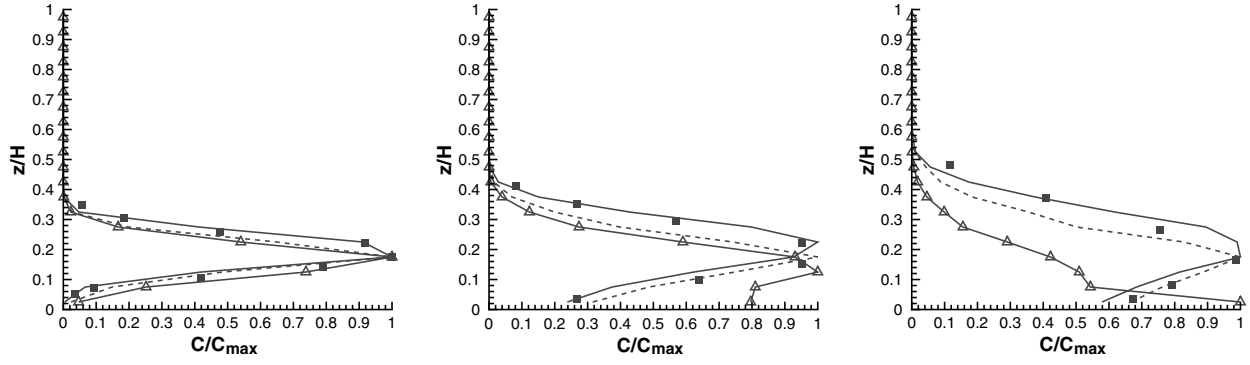

Fig. 4. Vertical profiles of mean concentration C at $x/H = 0.96$, $x/H = 1.92$ and $x/H = 2.88$—solid line: present simulation passive scalar; solid line connecting triangles: present simulation, droplets $d_p = 60$ μm; dashed line: present simulation, droplets 12 μm; squares: passive scalar, Fackrell and Robins (1982).

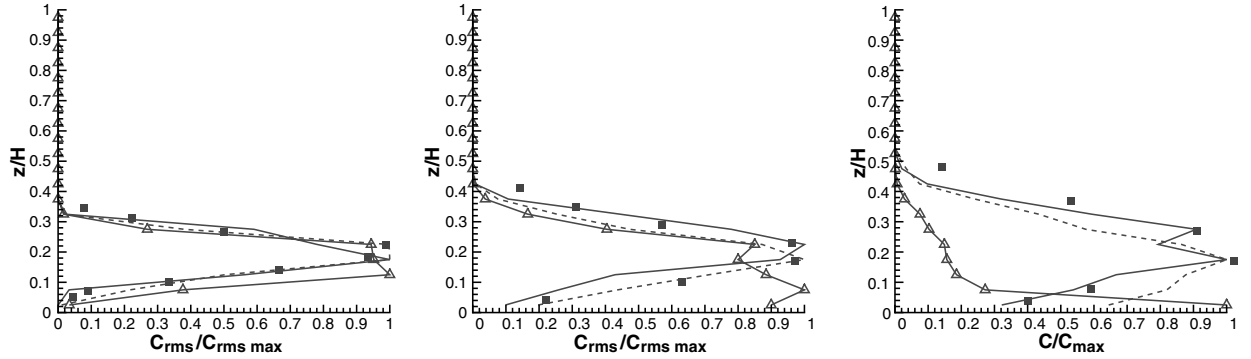

Fig. 5. Vertical profiles of mean-square concentration c' at $x/H = 0.96$, $x/H = 1.92$ and $x/H = 2.88$—solid line: present simulation passive scalar; solid line connecting triangles: present simulation, droplets $d_p = 60$ μm; dashed line: present simulation, droplets 12 μm; squares: passive scalar, Fackrell and Robins (1982).

Fig. 5 illustrates vertical profiles of mean-square concentration, c', for passive scalar and two sizes of droplets. As expected, the maximum value of the mean-square concentration for 60 μm droplets falls rapidly towards the ground. At the last station, even though the mean concentration profile for 12 μm droplets is similar to the concentration profile of a passive scalar, the mean-square concentration profiles differs significantly, specially close to the ground. This supports the fact that even if the mean concentration of small droplets presents the same behavior as a passive scalar plume, differences can remain for higher order moments.

Vertical profiles of vertical mass flux $\overline{w_p' c'}$, are illustrated in Fig. 6, where w_p' is the fluctuating vertical droplet velocity. The mass flux is normalized by the maximum concentration C_{max} and the friction velocity u_*. For both types of droplets, even close to the source mass fluxes differ from the passive scalar plume. Droplet mass flux profiles present a higher negative value close to the ground at $x/H = 0.96$, because, even for very small droplets sedimentation takes place. On the other hand, higher in the turbulent boundary layer, because of inertia, droplet mass flux profiles have lower peak values. We can also see that as the droplet diameter increases the peak value decreases.

In these simulations, the subgrid scale kinetic energy represents about 20% of the resolved kinetic energy as described in Vinkovic et al. (in press). Therefore, the subgrid stochastic model affects droplet dispersion as shown by the recent work of Pozorski et al. (2004) and in Vinkovic (2005).

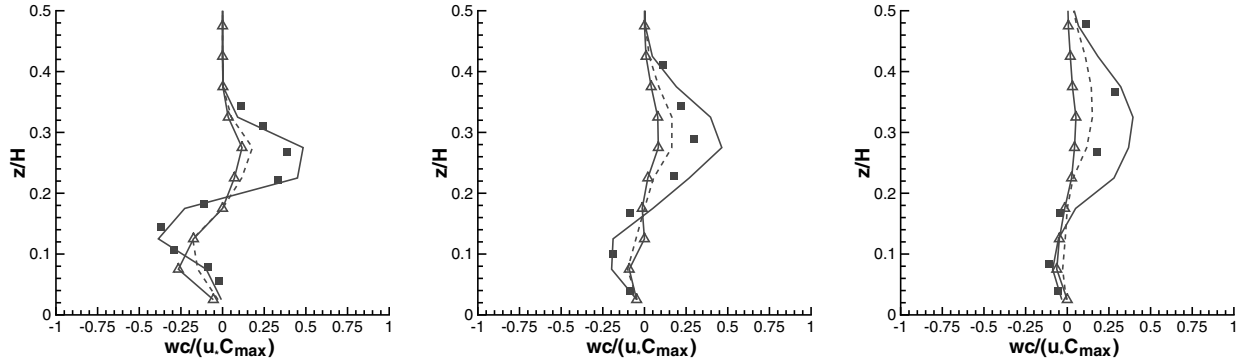

Fig. 6. Vertical flux $\overline{w_p' c'}$ at $x/H = 0.96$, $x/H = 1.92$ and $x/H = 2.88$—solid line: present simulation passive scalar; solid line connecting triangles: present simulation, droplets $d_p = 60$ μm; dashed line: present simulation, droplets 12 μm; squares: passive scalar, Fackrell and Robins (1982).

5.3. Coalescence and breakup of droplets within the wet cooling tower plume

In the previous section, the mean water content of the plume is fixed to 0.2 g/m^3, as measured by Hodin et al. (1980) in the plume of Bugey nuclear power plant. Because the water content is so low, the volume fraction of particles ($\Phi_p = 2\times10^{-7}$) is not high enough for collisions to be significant. As shown in Fig. 7, the relative velocities and the relative Weber numbers of droplets are such that coalescence can take place. However, no changes in the size distribution appear because of the low volume fraction.

In order to test the impact of coalescence, the number of 60 μm droplets per unit volume is increased up to a volume fraction of $\Phi_p = 2\times10^{-3}$. Fig. 8 illustrates the size distribution at different distances from the source. As the downstream distance increases, there is formation of bigger droplets. The changes in the size distribution are small. Compared to the initial Gaussian distribution we can notice that, here, the probability for having droplets with a diameter larger than 80 μm is no longer zero. Fig. 9 illustrates the vertical profile of mean concentration at three different downstream distances. Even though the changes in the size distribution are small, the mean concentration profile is modified. At $x = 0.96\delta$, the maximum concentration peak of the plume with a high volume fraction is closer to the ground than the maximum concentration peak of the plume with $\Phi_p = 2\times10^{-7}$. At $x = 1.92\delta$, the plume with the high volume fraction reaches the ground while the low level volume fraction plume remains suspended. Finally, at the last section, the dispersion of the plume with $\Phi_p = 2\times10^{-3}$ is smaller and this plume presents a higher concentration at the ground.

Fig. 10 illustrates vertical profiles of mean-square concentration for a plume with a volume fraction of $\Phi_p = 2\times10^{-3}$ compared to the plume studied in the section above. As expected, the profiles are modified.

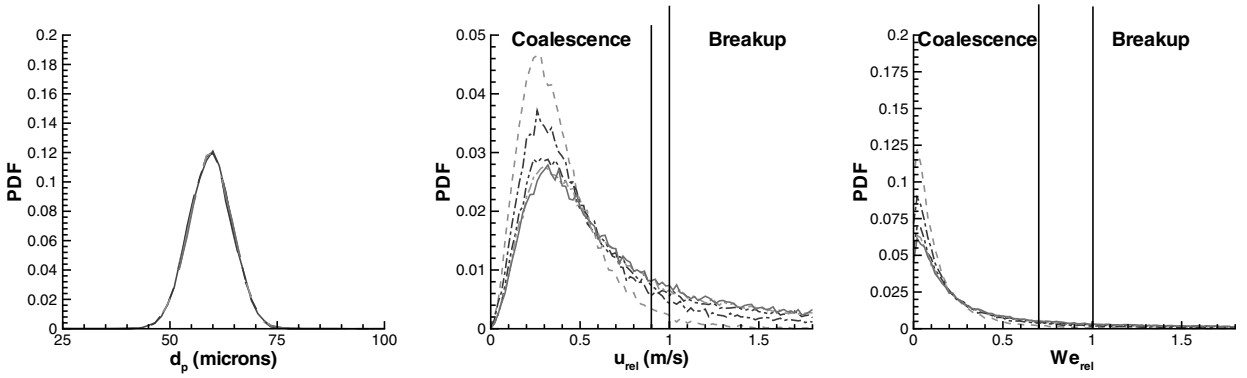

Fig. 7. Size distribution (left), relative velocity PDF (center) and PDF of relative Weber number (right) for 60 μm droplets and for $\Phi_p = 2\times10^{-7}$, at $x = 0.96\delta$, $x = 1.92\delta$, $x = 2.88\delta$, $x = 3.83\delta$ and $x = 4.79\delta$.

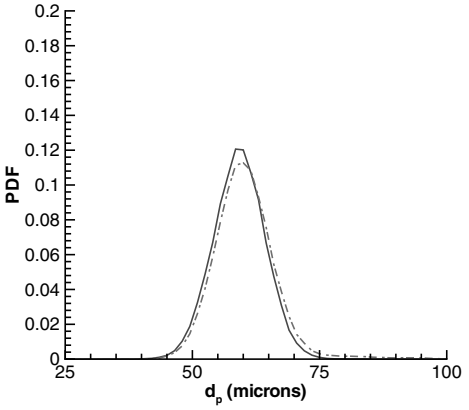

Fig. 8. Size distribution for 60 μm droplets and for $\Phi_p = 2\times10^{-3}$, at $x = 0.96\delta$ (full line) and $x = 4.79\delta$ (dashed line).

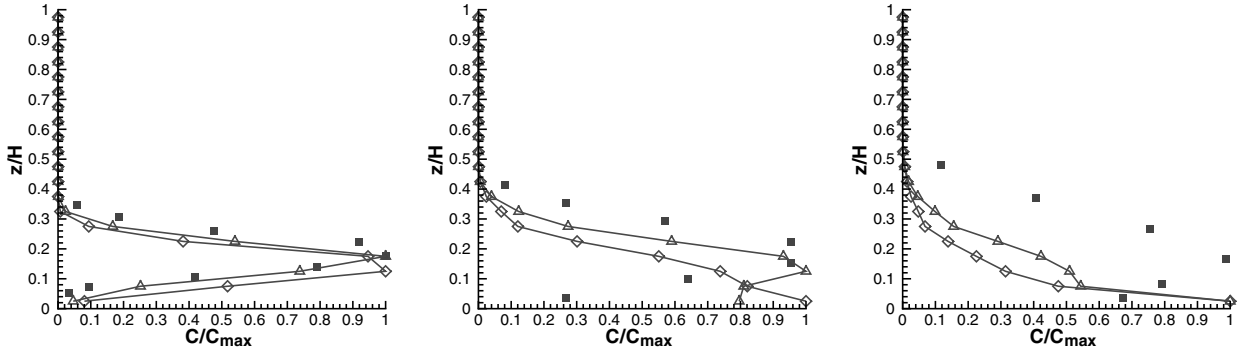

Fig. 9. Vertical profiles of mean concentration at $x/H = 0.96$, $x/H = 1.92$ and $x/H = 2.88$—solid line connecting triangles: present simulation, droplets $d_p = 60$ μm, $\Phi_p = 2 \times 10^{-7}$; solid line connecting diamonds: present simulation, droplets 60 μm, $\Phi_p = 2 \times 10^{-3}$; squares: passive scalar, Fackrell and Robins (1982).

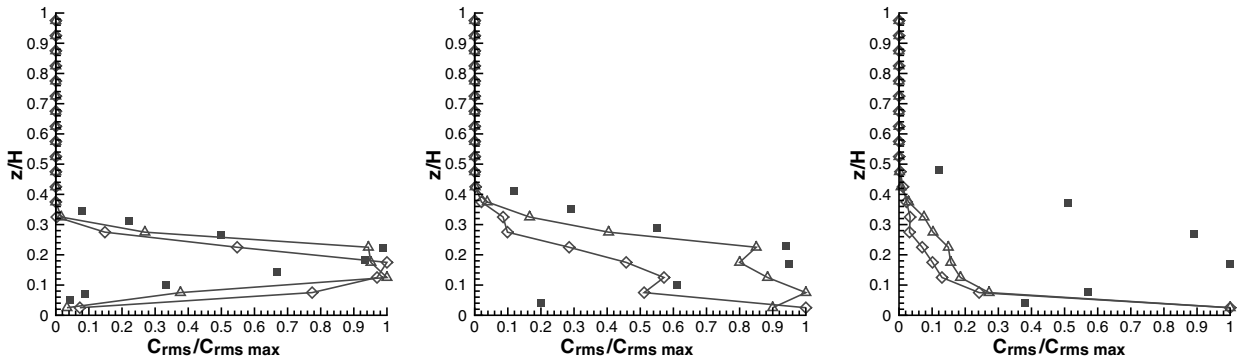

Fig. 10. Vertical profiles of mean-square concentration c' at $x/H = 0.96$, $x/H = 1.92$ and $x/H = 2.88$—solid line connecting triangles, present simulation, droplets $d_p = 60$ μm, $\Phi_p = 2 \times 10^{-7}$; solid line connecting diamonds: present simulation, droplets 60 μm, $\Phi_p = 2 \times 10^{-3}$; squares: passive scalar, Fackrell and Robins (1982).

The higher volume fraction plume reaches the ground faster, as can be seen from the mean-square concentration profiles where the maximum remains at the ground level.

Finally, the changes induced by the coalescence of droplets on the vertical mass flux profiles are shown in Fig. 11. As expected, when larger droplets appear in the plume, the mass flux near the ground becomes higher

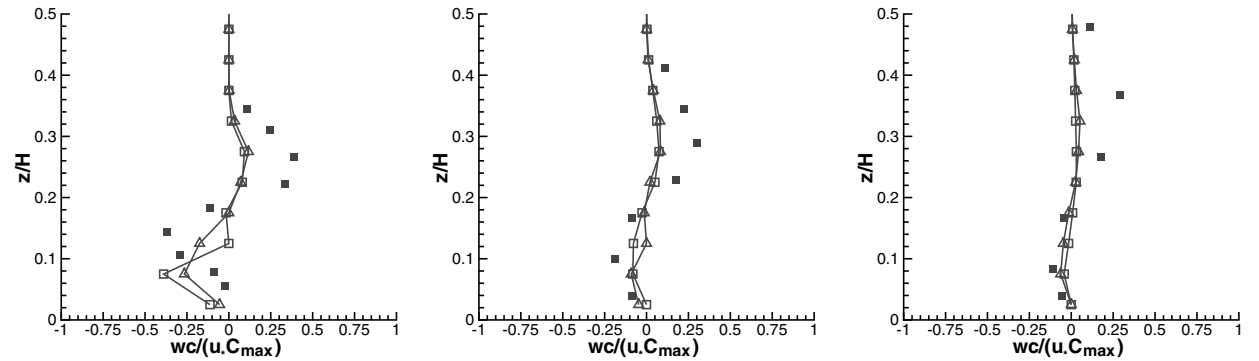

Fig. 11. Vertical flux $\overline{w'_p c'}$ at $x/H = 0.96$, $x/H = 1.92$ and $x/H = 2.88$—solid line connecting triangles: present simulation, droplets $d_p = 60$ μm, $\Phi_p = 2 \times 10^{-7}$; solid line connecting diamonds: present simulation, droplets 60 μm, $\Phi_p = 2 \times 10^{-3}$; squares: passive scalar, Fackrell and Robins (1982).

because of sedimentation and the mass flux, far from the ground, decreases because of sedimentation as well as of bigger particle inertia. Even small changes in the size distribution of a plume of droplets may produce important modification of the plume dispersion. Therefore, it is necessarily to describe and model correctly all interaction that may lead to changes in droplet size.

The model for coalescence and breakup presented here (Section 3) was applied to the splashing of droplets during impact on the wall. The relative velocity between a pair of droplets was replaced by the velocity of the droplet impacting the wall. Whether this model is applied or not has no influence on the results because the droplets reaching the wall do not have enough velocity to splash.

6. Conclusion

A LES with the dynamic SGS model of Germano et al. (1991) coupled with a Lagrangian stochastic model has been applied to the study of droplet dispersion in a turbulent boundary layer. Droplets are tracked in a Lagrangian way. The velocity of the fluid particle along the droplet trajectory is considered to have a large-scale part and a small-scale part given by a modified three-dimensional Langevin model using the filtered SGS statistics. An appropriate Lagrangian correlation timescale is considered in order to include the influences of gravity and inertia. Two-way coupling is also taken into account.

A model for droplet coalescence and breakup has been implemented which allows to predict droplet interactions under turbulent flow conditions in the frame of the Euler/Lagrange approach. Coalescence and breakup are considered in the framework of stochastic process with simple scaling symmetry assumption for the droplet radius. At high-frequency of breakup/coalescence phenomena, this stochastic process is equivalent to the evolution of the PDF of droplet radii, which is governed by a Fokker–Planck equation. The parameters of the model are obtained dynamically by relating them to the local resolved properties of the dispersed phase compared to the mean fluid. Within each grid cell, mass conservation is applied. The model is validated by comparison with the agglomeration model of Ho and Sommerfeld (2002) and the experimental results on secondary breakup of Lasheras et al. (1998). The critical parameters of our model are fixed in order to fit the time evolution of the size distribution of Ho and Sommerfeld (2002). Natural droplet contact is introduced by the particle pairing process for collision.

The LES coupled with Lagrangian particle tracking and the model for droplet coalescence and breakup is applied to the study of the atmospheric dispersion of wet cooling tower plumes. Since we did not find any wind tunnel experiment or in-situ measurements of droplet dispersion in an atmospheric turbulent boundary layer we compared the numerical results with the experiment on passive scalar plume dispersion of Fackrell and Robins (1982). The simulations are done for two different droplet size distributions (60 μm and 12 μm) and for two volume fractions ($\Phi_p = 2 \times 10^{-7}$ and $\Phi_p = 2 \times 10^{-3}$).

Both types of droplets fall to the ground faster than the passive scalar plume. Far from the source, droplets of 12 μm remain suspended while 60 μm droplets present a maximum concentration at the ground. Even if the mean concentration of small droplets presents the same mean behavior as a passive scalar plume, differences can remain for higher order moments. For both types of droplets, even close to the source mass fluxes differ from the passive scalar plume. Droplet mass flux profiles present a higher negative value close to the ground at $x/H = 0.96$, because, even for very small droplets, sedimentation takes place. On the other hand, higher in the turbulent boundary layer, because of inertia, droplet mass flux profiles have lower peak values. As the droplet diameter increases this peak value decreases.

When the volume fraction of droplets in the plume is increased, coalescence takes place. Even though the changes in the size distribution are small, the mean concentration profile is modified. The high volume fraction plume reaches the ground faster, it is less dispersed and it presents a higher concentration at the ground. When larger droplets appear in the plume, the mass flux near the ground becomes higher the mass flux far from the ground decreases because of sedimentation bigger particle inertia, respectively. Even small changes in the size distribution of a plume of droplets may produce important modification of the plume dispersion. Therefore, it is necessarily to describe and model correctly all interaction that may lead to changes in droplet size.

Further developments will tend to introduce chemical reactions between droplets and evaporation. Another objective is to unify the LES with particle tracking of droplets, with the LES with passive and reactive scalar

dispersion as well as with solid particles. This should ultimately provide a physically sound and efficient tool for computation of atmospheric chemistry and aerosol dispersion and interaction.

References

Aguirre, C., Guo, Y., Ayrault, M., 2004. Dispersion de particules solides en mouvement de saltation dans un écoulement turbulent. C. R. Acad. Sci. 332, 627–632.

Apte, S.V., Gorokhovski, M., Moin, P., 2003. LES of atomizing spray with stochastic modeling of secondary breakup. Int. J. Multiphase Flow 29, 1503–1522.

Ashgriz, N., Poo, J.Y., 1990. Coalescence and separation in binary collisions of liquid drops. J. Fluid Mech. 221, 183–204.

Boivin, M., Simonin, O., Squires, K.D., 1998. Direct numerical simulation of turbulence modulation by particles in isotropic turbulence. J. Fluid Mech. 375, 235–263.

Brazier-Smith, P.R., Jennings, S.G., Latham, J., 1972. The interaction of falling water drops: coalescence. Proc. R. Soc. Lond. A 326, 393–408.

Casulli, V., Cheng, R.T., 1992. Semi-implicit finite difference methods for the three-dimensional shallow water flow. Int. J. Numer. Methods Fluids 15, 629–648.

Clift, R., Grace, J.R., Weber, M.E., 1978. Bubbles, Drops and Particles. Academic Press, New York.

Csanady, G.T., 1963. Turbulent diffusion of heavy particles in the atmosphere. J. Atmos. Sci. 20, 201–208.

Deardorff, J.W., 1970. A numerical study of three-dimensional turbulent channel flow at large Reynolds numbers. J. Fluid Mech. 41, 453–480.

Deardorff, J.W., 1980. Stratocumulus-capped mixed layer derived from a three dimensional model. Bound.-Lay. Meteorol. 18, 495–527.

Durbin, P.A., 1983. Stochastic differential equations and turbulent dispersion. NASA Reference Publication 1103.

Fackrell, J.E., Robins, A.G., 1982. Concentration fluctuations and fluxes in plumes from point sources in a turbulent boundary layer. J. Fluid Mech. 117, 1–26.

Fukagata, K., Zahrai, S., Bark, F.H., 1998. Force balance in a turbulent particulate channel flow. Int. J. Multiphase Flow 24, 867–887.

Gardiner, C.W., 1985. Handbook of Stochastic Methods, second ed. Springer-Verlag.

Georjon, T.L., Reitz, R.D., 1999. A drop-shattering collision model for multidimensional spray computations. J. Atomizat. Sprays 9, 231–254.

Germano, M., Piomelli, U., Moin, P., Cabot, W.H., 1991. A dynamic subgridscale viscosity model. Phys. Fluids 3, 1760–1765.

Ghosal, S., Lund, T.S., Moin, P., Akselvoll, K., 1995. A dynamic localization model for large-eddy simulation of turbulent flows. J. Fluid Mech. 286, 229–255.

Gorokhovski, M.A., 2001. The stochastic subgrid scale approach for spray atomization. J. Atomizat. Sprays 11, 505–519.

Gorokhovski, M.A., Saveliev, V.L., 2003. Analysis of Kolmogorov's model of breakup and its application into Lagrangian computation of liquid sprays under air-blast atomization. Phys. Fluids 15, 184–192.

Ho, C.A., Sommerfeld, M., 2002. Modelling of micro-particle agglomeration in turbulent flows. Chem. Eng. Sci. 57, 3073–3084.

Hodin, A., Mery, P., Saab, A., 1980. Meteorological influence of wet cooling tower plumes: its measurements, modelling, and forecasting. Rapport EDF 32-80.21.

Klemp, J.B., Wilhelmson, R., 1978. The simulation of three-dimensional convective storms dynamics. J. Atmos. Sci. 35, 1070–1096.

Kollár, L.E., Farzaneh, M., Karev, A.R., 2005. Modeling droplet collision and coalescence in an icing wind tunnel and the influence of these processes on droplet size distribution. Int. J. Multiphase Flow 31, 69–92.

Kolmogorov, A.N., 1941. On the log-normal distribution of particles sizes during breakup process. Dokl. Akad. Nauk. SSSR 31, 99–101.

Lasheras, J.C., Villermaux, E., Hopfinger, E.J., 1998. Break-up and atomization of a round water jet by a high-speed annular air jet. J. Fluid Mech. 357, 351–379.

Lilly, D.K., 1992. A proposed modification of the Germano subgrid-scale closure method. Phys. Fluids 4, 633–635.

Mashayek, F., Pandya, R.V., 2003. Analytical description of two-phase turbulent flows. Prog. Energy Combust. Sci. 29, 329–378.

Meeder, J.P., Nieuwstadt, F.T.M., 2000. Large-eddy simulation of the turbulent dispersion of a reactive plume from a point source into a neutral atmospheric boundary layer. Atmos. Environ. 34, 3563–3573.

Meneveau, C., Katz, J., 2000. Scale-invariance and turbulence model for large-eddy simulation. Annu. Rev. Fluid Mech. 32, 1–32.

Orme, M., 1997. Experiments on droplet collisions, bounce, coalescence and disruption. Prog. Energy Combust. Sci. 23, 65–79.

Pan, Y., Banerjee, S., 1996. Numerical simulation of particle interactions with wall turbulence. Phys. Fluids 8, 2733–2755.

Porahmadi, F., Humphrey, J.A.C., 1983. Modeling solid turbulent flows. Phys. Chem. Hydrodyn., 191–219.

Pozorski, J., Minier, J.P., 1998. On the Lagrangian turbulent dispersion models based on the Langevin equation. Int. J. Multiphase Flow 24, 913–945.

Pozorski, J., Apte, S.V., Raman, V., 2004. Filtered particle tracking for dispersed two-phase turbulent flows. In: Proceedings of the Summer Program 2004, Center for Turbulence Research, pp. 329–340.

Qian, J., Law, C.K., 1997. Regimes of coalescence and separation in droplet collision. J. Fluid Mech. 331, 59–80.

Reynolds, A.M., 2000. On the formulation of Lagrangian stochastic models for heavy-particle trajectories. J. Colloid. Int. Sci. 232, 260–268.

Rodgers, C.B., Eaton, J.K., 1990. The behavior of solid particles in a vertical turbulent boundary layer. Int. J. Multiphase Flow 16, 819–834.

Sawford, B.L., Guess, F.M., 1991. Lagrangian statistical simulation of the turbulent motion of heavy particles. Bound.-Lay. Meteorol. 54, 147–166.

Shao, Y., 1995. The fractional Ornstein-Uhlenbeck process as a representation on the entrainment of dust by wind. Physica D 83, 461–477.

Shao, Y., Li, A., 1999. Numerical modeling of saltation in the atmospheric surface layer. Bound.-Lay. Meteorol. 91, 199–225.

Sommerfeld, M., 2001. Validation of a stochastic Lagrangian modelling approach for inter-particle collisions in homogeneous isotropic turbulence. Int. J. Multi-phase Flow 27, 1829–1858.

Stock, D.E., 1996. Particle dispersion in flowing gases. J. Fluids Eng. 118, 4–17.

Sykes, R.I., Henn, D.S., 1992. Large-eddy simulation of the concentration fluctuations in a dispersing plume. Atmos. Environ. 26A, 3127–3144.

Sykes, R.I., Henn, D.S., Parker, S.F., 1992. Large-eddy simulation of a turbulent reacting plume. Atmos. Environ. 26A, 2565–2574.

Thomson, D.J., 1987. Criteria for the selection of stochastic models of particle trajectories in turbulent flows. J. Fluid Mech. 180, 529–556.

van Dop, H., Nieuwstadt, F.T.M., Hunt, J.C.R., 1986. Random walk models for particle displacement in inhomogeneous unsteady turbulent flows. Phys. Fluids 28, 1639–1653.

Vinkovic, I., 2005. Dispersion et mélange turbulents de particules solides et de gouttelettes par une simulation des grandes échelles et une modélisation stochastique lagrangienne. Ph.D. Thesis, Ecole Centrale de Lyon.

Vinkovic, I., Aguirre, C., Simoëns, S., in press. Large-eddy simulation and Lagrangian stochastic modeling of passive scalar dispersion in a turbulent boundary layer. J. Turbul.

Vinkovic, I., Aguirre, C., Simoëns, S., Gence, J.N., 2005a. Coupling of a subgrid Lagrangian stochastic model with large-eddy simulation. C. R. Mecanique 333, 325–330.

Vinkovic, I., Ayrault, M., Simoëns, S., Aguirre, C., 2005b. Large eddy simulation of the dispersion of solid particles in a turbulent boundary layer. TSFP4, Williamsburg, VA, USA.

Wang, Q., Squires, K.D., 1996a. Large eddy simulation of particle deposition in a vertical turbulent channel flow. Int. J. Multiphase Flow 22, 667–683.

Wang, Q., Squires, K.D., 1996b. Large eddy simulation of particle-laden turbulent channel flow. Phys. Fluids 8, 1207–1223.

Xie, Z., Hayden, P., Voke, R., Robins, A.G., 2004. Large-eddy simulation of dispersion: comparison between elevated and ground-level sources. J. Turbul. 5, 1–16.

Xue, M., Droegemeier, K.K., Wong, V., 2000. The Advanced Regional Prediction System (ARPS)—a multi-scale nonhydrostatic atmospheric simulation and prediction model. Part I: Model dynamics and verification. Meteorol. Atmos. Phys. 75, 161–193.

Xue, M., Droegemeier, K.K., Wong, V., Shapiro, A., Brewster, K., Carr, F., Weber, D., Liu, Y., Wang, D., 2001. The Advanced Regional Prediction System (ARPS)—a multi-scale nonhydrostatic atmospheric simulation and prediction tool. Part II: Model physics and applications. Meteorol. Atmos. Phys. 76, 143–165.

Zhuang, Y., Wilson, J.D., Lozowski, E.P., 1989. A trajectory-simulation model for heavy particle motion in turbulent flow. Trans. ASME, J. Fluid Eng. 111, 492–494.